

Article

Robust LQR Design Method for the Aero-Engine Integral Constant Pressure Drop Control Valve with High Precision

Wenshuai Zhao ^{1,*}, Xi Wang ¹, Yifu Long ¹, Zhenhua Zhou ² and Linhang Tian ²

¹ School of Energy and Power Engineering, Beijing University of Aeronautics and Astronautics, Beijing 100191, China; xwang@buaa.edu.cn (X.W.); lyfleo@buaa.edu.cn (Y.L.)

² AECC Guizhou Honglin Aeroengine Control Technology Co., Ltd., Guiyang 550009, China

* Correspondence: m13716752318_1@163.com

Abstract: The closed-loop constant pressure drop control valve is widely used in aero-engine fuel servo metering systems. However, the available constant pressure drop control valve cannot realize servo tracking without static error and, often, a high proportional gain is used to reduce the static error and improve the servo tracking performance, which reduces the stability margin. In this paper, an integral constant pressure drop control valve is designed, which consists of an integral controller and a stabilizing controller. Moreover, a robust LQR design method is proposed to complete the design task. Firstly, the controlled plant's state-space model is derived, and the augmented model with tracking error is established based on the robust servo system design theory. Secondly, a servo controller with dual functions of integral control and stabilization control is constructed and decoupled, in which the stabilizing controller guarantees the asymptotic stability as well as the anti-disturbance performance, and the integral controller realizes the servo tracking without static error. Finally, based on the robust LQR design method, two key design parameters, including the integral control gain and the stabilization control gain, are designed to complete the design task. The simulation results indicate that, even when suffering 50 mm² metered flow area step disturbance and 1 MPa inlet pressure step change, the designed integral constant pressure drop control valve can realize the function of servo tracking without static error. The static error is almost 0, the settling time is within 0.01 s, the overshoot is within 10%, and the phase margin is more than 55°.



Citation: Zhao, W.; Wang, X.; Long, Y.; Zhou, Z.; Tian, L. Robust LQR Design Method for the Aero-Engine Integral Constant Pressure Drop Control Valve with High Precision.

Aerospace **2023**, *10*, 428. <https://doi.org/10.3390/aerospace10050428>

Academic Editor: Jian Liu

Received: 9 March 2023

Revised: 25 April 2023

Accepted: 26 April 2023

Published: 30 April 2023



Copyright: © 2023 by the authors. Licensee MDPI, Basel, Switzerland. This article is an open access article distributed under the terms and conditions of the Creative Commons Attribution (CC BY) license (<https://creativecommons.org/licenses/by/4.0/>).

Keywords: aero-engine fuel servo metering system; integral constant pressure drop control valve; servo tracking without static error; integral controller; stabilizing controller; robust LQR design method

1. Introduction

The aero-engine fuel servo metering system basically adopts the constant pressure drop control principle to complete fuel metering, except for very few applications of the variable pressure drop control structure, such as the fuel regulator in the Spey MK202 turbofan engine in the Rolls-Royce [1]. However, the available constant pressure drop control valve cannot realize servo tracking without static error and, often, a high proportional gain is used to reduce the static error and improve the servo tracking performance. The control theory explains that if there is no integral part in the closed-loop system, but only a proportional part, then the closed-loop system exhibits static error under any circumstances [2,3]. Although the high proportional gain can reduce the static error, it reduces the system stability and, even, causes aero-engine instability in the acceleration and deceleration process, such as thrust and speed swing [4]. In addition, as the high precision, high stability, and high robustness requirements in the modern aero-engine control system are proposed, it is crucial to improve the servo tracking ability and robustness of the constant pressure drop control valve.

Early studies about the constant pressure drop control valve primarily concentrated on frequency domain modeling and analysis. Specifically, based on the derived frequency

domain models, the steady-state and dynamic characteristics of the whole system, as well as the stability variation under different structure parameters, were analyzed [5–7]. These studies offer some basic methods, however, due to the limitations to classical control theory and simulation technology, the established models are complex, the proposed methods cannot explain the design theory, and the conclusions cannot be verified because of lacking simulation works. In recent years, simulation technology has developed rapidly, and many studies relying on simulation technology have appeared, mainly concentrating on nonlinear modeling and simulation. For example, when the structure parameter values change, such as the hole diameter and the spring stiffness, the system performance variations are analyzed and simulated, and some guidance on the design structure parameters is offered [8–12]. However, these studies lack theoretical analysis and only rely on nonlinear simulation, causing difficulty in guiding the design process. Moreover, relying on the transfer function models, the system's stability conditions are analyzed [13]. Indeed, the analysis results should be confirmed, because the model is oversimplified, and the study lacks a simulation comparison. Besides, some detailed studies, concentrating on the system's characteristic changes with the return orifice profile structure, explain the correlation between the profile structure and the system control gain [14–16]. Nevertheless, these studies have limitations, because they only offer guidance for orifice profile design, rather than system design. Furthermore, there are some unique studies. For example, an ideal variable orifice is constructed and tested physically, and the test results indicate that the variable structure can enhance system performance [17]. Despite lacking design theory analysis, the design idea for the variable orifice structure in this study is helpful. In addition, through CFD simulation, the valve balance characteristic related to the flow force are explored [18–21]. The conclusions indicate that the flow force will affect the system performance, but it is not the most crucial aspect. Moreover, some physical tests have been executed to explore the influence of hysteresis on the speed fluctuation [22,23]. However, the theoretical analysis and results discussion in these studies are unclear, and they do not involve the design process. A new remarkable study, using the linear incremental analysis method, reveals the design theory for a constant pressure drop control valve, and proposes the frequency domain analysis and design methods, realizing a pretty good performance [24]. The study proposes efficient guidance measures and design methods; however, it is still limited to classical control design methods, and cannot realize servo tracking without static error.

These studies concentrate on classical control theory, rather than modern control theory, to study the high proportional gain constant pressure drop control valve, causing complex analysis and design processes. With the design object of servo tracking without static error, this paper uses the modern servo control theory to complete the design of the constant pressure drop control valve with static error-free tracking capability and provides a technical approach that can be used in engineering for high precision fuel metering. This paper makes the following contributions:

1. Firstly, based on the modern servo model design theory, an integral design structure for the constant pressure drop control valve is proposed, and a servo controller with dual functions of integral control and stabilization control is constructed;
2. Secondly, based on the decoupling design theory, the servo controller is decoupled. Where the stabilizing controller guarantees the asymptotic stability, as well as the disturbance rejection performance, and the integral controller realizes the command servo tracking without static error;
3. Finally, a robust LQR design method is proposed to design the control gains of the system, and it completes the design task well. The method is proven to guarantee fine performance and stability, as well as strong robust performance.

The chapters are arranged as follows. In Section 2, an integral design structure is constructed and the relevant design theory is derived. In Section 3, the servo controller is decoupled and realized. In Section 4, a robust LQR design method is proposed, and

the design and implementation processes for the system are given. In Section 5, a design example is provided. In Section 6, the conclusions are presented.

2. Theoretical Design

A typical fuel metering system structure is shown in Figure 1. In general, the fuel flow metering equation is represented as $Q = C_q A \sqrt{2\Delta P / \rho}$, in which the pressure drop ΔP is designed as a constant, and the required fuel flow Q is metered by the metered flow area A [13,24]. Specifically, the pressure drop control valve is used to guarantee the constant pressure drop ΔP , and the fuel metering valve is used to realize the control of the metered flow area A .

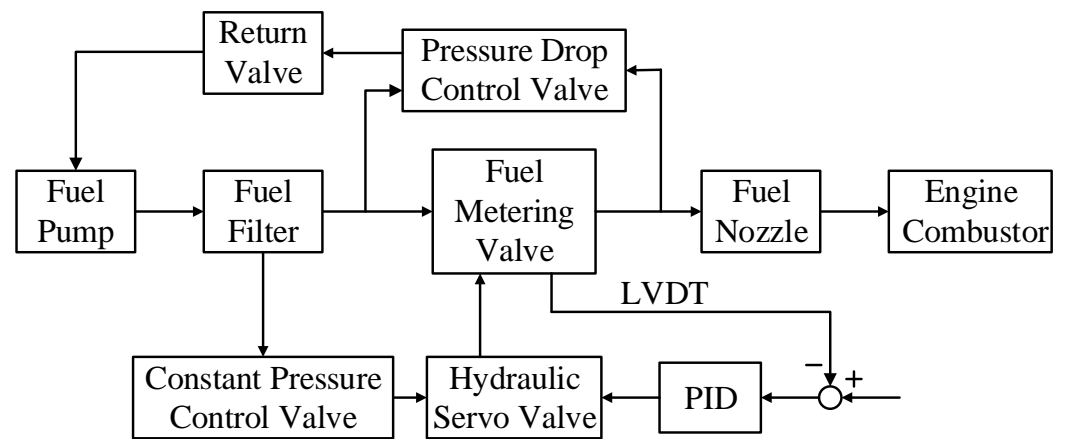


Figure 1. Structure diagram of the fuel metering system.

This paper concerns the design problem of the pressure drop control valve. The designed integral constant pressure drop control valve is shown in Figure 2, which is improved from the general pressure drop control valve [12,24].

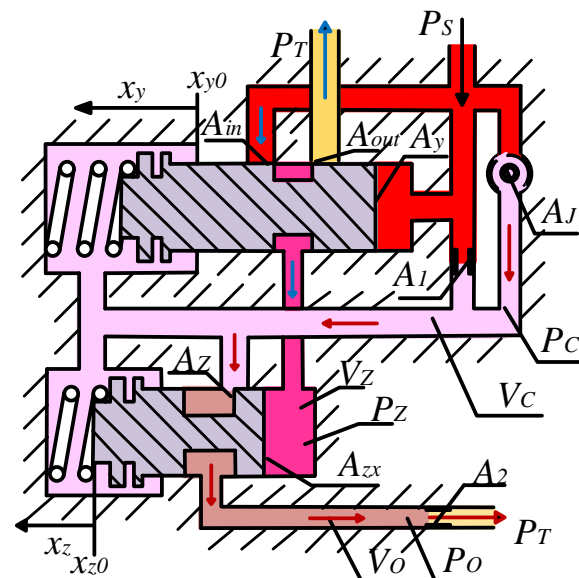


Figure 2. Structure diagram of the integral constant pressure drop control valve.

The parameters are defined as follows: P_S is the inlet pressure, P_T is the return pressure, P_C is the controlled pressure, P_Z is the adjusting pressure, P_O is the ejection pressure; A_J is the metered flow area, A_{in} is the servo inlet flow area, A_{out} is the servo outlet flow area, A_Z is the adjusting flow area, A_1 is the fixed inlet flow area, A_2 is the fixed ejection flow area; V_C is the controlled chamber volume, V_Z is the adjusting chamber volume, V_O is

the ejection chamber volume; x_z is the adjusting valve displacement, x_y is the servo valve displacement; A_y is the servo valve pressure bearing area, and A_{zx} is the adjusting valve pressure bearing area [24].

2.1. Working Principle

For the integral constant pressure drop control valve, the fuel flow metering equation is correspondingly represented as $Q = C_q A_J \sqrt{2(P_S - P_C)/\rho}$, in which the pressure drop is $(P_S - P_C)$, and the metered flow area is A_J .

Generally, for the pressure drop control valve, the metered flow area A_J is considered as the disturbance input and the inlet pressure P_S is considered as the reference input, and the working principle of the system is described as: when the metered flow area A_J disturbs or the inlet pressure P_S changes, the controlled pressure P_C changes, and the pressure drop $(P_S - P_C)$ deviates from the designed value. Instantaneously, because the pressure drop $(P_Z - P_C)$ changes, the adjusting valve moves and the adjusting flow area A_Z changes, realizing a rapid regulation of the P_C . Simultaneously, because the pressure drop $(P_S - P_C)$ changes, the servo valve also moves and the servo inlet and outlet flow area A_{in} and A_{out} change, realizing a precise regulation of the P_C . The dual function restores the pressure drop $(P_S - P_C)$ to the design value [24–30].

Hence, the design objective is to ensure the controlled pressure P_C servo tracks the inlet pressure P_S without static error, and rejects the disturbance related to the metered flow area A_J .

2.2. State–Space Model of the Controlled Plant

The controlled plant is composed of the controlled pressure and the ejection pressure, and their pressure–flow nonlinear dynamic equations are:

$$\frac{dP_C}{dt} = \frac{B}{V_C} \cdot \left((C_{q1}A_1 + C_{qj}A_J) \sqrt{\frac{2(P_S - P_C)}{\rho}} - C_{qz}A_Z \sqrt{\frac{2(P_C - P_O)}{\rho}} + A_y \dot{x}_y + A_{zx} \dot{x}_z \right) \tag{1}$$

$$\frac{dP_O}{dt} = \frac{B}{V_O} \cdot \left(C_{qz}A_Z \sqrt{\frac{2(P_C - P_O)}{\rho}} - C_{qo}A_2 \sqrt{\frac{2(P_O - P_T)}{\rho}} \right) \tag{2}$$

where ρ is the oil density, B is the oil bulk modulus, and C_q is the flow coefficient.

The calculation formula for C_q is:

$$C_q = C_{qmax} \cdot \tanh\left(\sqrt{\frac{8|\Delta P|}{\rho}} \cdot \frac{\rho \cdot d_h}{Nu \cdot lamc}\right) \tag{3}$$

where C_{qmax} is the maximum flow coefficient, d_h is the hydraulic diameter, Nu is the absolute viscosity, and $lamc$ is the critical flow number [24].

The relevant linear dynamic differential equations are:

$$\Delta \dot{P}_C = \frac{B}{V_C} \cdot \left(-(K_{PJ} + K_{PZ}) \cdot \Delta P_C + K_{PZ} \cdot \Delta P_O + K_{PJ} \cdot \Delta P_S + K_{AJ} \cdot \Delta A_J - K_{AZ} \cdot \Delta A_Z + A_{zx} \cdot \Delta \dot{x}_z + A_y \cdot \Delta \dot{x}_y \right) \tag{4}$$

$$\Delta \dot{P}_O = \frac{B}{V_O} \cdot \left(-(K_{PZ} + K_{PT}) \cdot \Delta P_O + K_{PZ} \cdot \Delta P_C + K_{AZ} \cdot \Delta A_Z \right) \tag{5}$$

where $K_{AJ} = C_{qj} \sqrt{\frac{2(P_S - P_C)}{\rho}}$, $K_{AZ} = C_{qz} \sqrt{\frac{2(P_C - P_O)}{\rho}}$, $K_{PZ} = C_{qz} A_Z \sqrt{\frac{1}{2\rho(P_C - P_O)}}$, $K_{PT} = C_{qo} A_2 \sqrt{\frac{1}{2\rho(P_O - P_T)}}$, $K_{PJ} = (C_{qj} A_J + C_{q1} A_1) \sqrt{\frac{1}{2\rho(P_S - P_C)}}$.

Finally, the state–space model of the controlled plant is:

$$\begin{aligned} \dot{x}_p &= A_p x_p + B_p u_p + E_p w \\ y_p &= C_p x_p + D_p u_p \end{aligned} \tag{6}$$

where $x_p = [\Delta P_C \ \Delta P_O]^T, u_p = [\Delta A_Z \ \Delta \dot{x}_y \ \Delta \dot{x}_z]^T, w = [\Delta A_J \ \Delta P_S]^T, y_p = [\Delta P_C \ \Delta P_O]^T,$

$$A_p = \begin{bmatrix} -\frac{B}{V_C} \cdot (K_{PJ} + K_{PZ}) & \frac{B}{V_C} \cdot K_{PZ} \\ \frac{B}{V_O} \cdot K_{PZ} & -\frac{B}{V_O} \cdot (K_{PZ} + K_{PT}) \end{bmatrix}$$

$$B_p = \begin{bmatrix} -\frac{B}{V_C} \cdot K_{AZ} & \frac{B}{V_C} \cdot A_y & \frac{B}{V_C} \cdot A_{zx} \\ \frac{B}{V_O} \cdot K_{AZ} & 0 & 0 \end{bmatrix}, E_p = \begin{bmatrix} \frac{B}{V_C} \cdot K_{AJ} & \frac{B}{V_C} \cdot K_{PJ} \\ 0 & 0 \end{bmatrix} \quad (7)$$

$$C_p = \begin{bmatrix} 1 & 0 \\ 0 & 1 \end{bmatrix}, D_p = \begin{bmatrix} 0 & 0 & 0 \\ 0 & 0 & 0 \end{bmatrix}$$

2.3. Structure Design of the Servo Controller

As mentioned previously, the adjusting flow area A_Z is regarded as the main control input. Considering the controlled pressure P_C as the output feedback variable, according to the robust servo system design theory, as well as the steady-state deviation design method [2,3], the theoretical design diagram of the control architecture is shown in Figure 3.

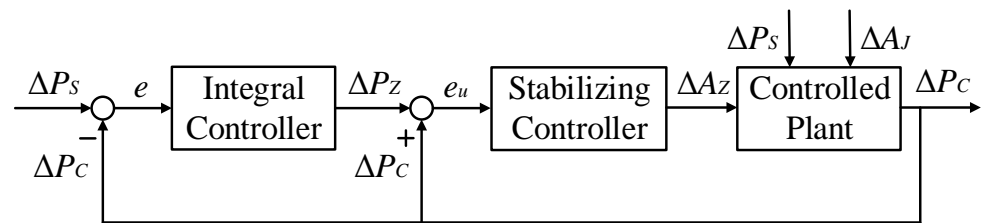


Figure 3. Theoretical design diagram of the control architecture.

Correspondingly, the design objective is to ensure the controlled pressure increment ΔP_C servo tracks the inlet pressure increment ΔP_S without static error, and rejects the disturbance related to the metered flow area increment ΔA_J . The detailed design processes are detailed below.

The tracked input signal ΔP_S and the rejected disturbance signal ΔA_J are both constant value signals, and their first order differential equations are expressed as $\Delta \dot{A}_J = 0$ and $\Delta \dot{P}_S = 0$, respectively. Since the input signals are constant, an integrator needs to be added to realize servo tracking without static error.

The tracking error signal is defined as:

$$e = \Delta P_C - \Delta P_S \quad (8)$$

Then, the first order differential equation of the tracking error signal is:

$$\dot{e} = \Delta \dot{P}_C \quad (9)$$

A new state vector is defined as:

$$z = [e \ \xi]^T \quad (10)$$

The augmented servo system design model is:

$$\dot{z} = \tilde{A}z + \tilde{B}\mu \quad (11)$$

where $\xi = \dot{x}_p = [\Delta \dot{P}_C \ \Delta \dot{P}_O]^T, \mu = \dot{u}_p = [\Delta \dot{A}_Z \ \Delta \ddot{x}_y \ \Delta \ddot{x}_z]^T,$ and

$$\tilde{A} = \begin{bmatrix} 0 & 1 & 0 \\ 0 & -\frac{B}{V_C} \cdot (K_{PJ} + K_{PZ}) & \frac{B}{V_C} \cdot K_{PZ} \\ 0 & \frac{B}{V_O} \cdot K_{PZ} & -\frac{B}{V_O} \cdot (K_{PZ} + K_{PT}) \end{bmatrix}, \tilde{B} = \begin{bmatrix} 0 & 0 & 0 \\ -\frac{B}{V_C} \cdot K_{AZ} & \frac{B}{V_C} \cdot A_y & -\frac{B}{V_C} \cdot A_{zx} \\ \frac{B}{V_O} \cdot K_{AZ} & 0 & 0 \end{bmatrix} \quad (12)$$

The output feedback vector is defined as $y_c = [e \quad \Delta\dot{P}_C]^T$, and the output model is:

$$y_c = \tilde{C}z + \tilde{D}\mu \tag{13}$$

where $\tilde{C} = \begin{bmatrix} 1 & 0 & 0 \\ 0 & 1 & 0 \end{bmatrix}$, $\tilde{D} = \begin{bmatrix} 0 & 0 & 0 \\ 0 & 0 & 0 \end{bmatrix}$.

Then, the output feedback control law of the servo model is:

$$\mu = -K_c \cdot y_c = -[k_1 \quad k_2] \begin{bmatrix} e \\ \Delta\dot{P}_C \end{bmatrix} = -(k_1 e + k_2 \Delta\dot{P}_C) \tag{14}$$

where k_1 and k_2 are the elements of the output feedback control gain vector K_c .

Then, the control input of the controlled plant can be expressed as:

$$\begin{aligned} u &= \int \mu dt \\ &= -\int (k_1 \cdot e + k_2 \cdot \Delta\dot{P}_C) dt \\ &= -k_1 \cdot \int e dt - k_2 \cdot \Delta P_C \end{aligned} \tag{15}$$

Represented by the physical control input ΔA_Z , it has:

$$\begin{aligned} \Delta A_Z &= -k_1 \cdot \int (\Delta P_C - \Delta P_S) dt - k_2 \cdot \Delta P_C \\ &= k_2 \cdot \left(\frac{k_1}{k_2} \cdot \int (\Delta P_S - \Delta P_C) dt + \Delta P_C \right) \end{aligned} \tag{16}$$

The specific structure design diagram of the servo controller is shown in Figure 4.

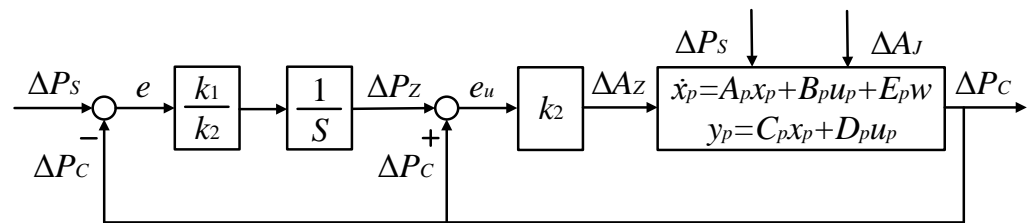


Figure 4. Structure design diagram of the servo controller.

Since the above servo controller is coupled, it cannot be directly realized in a hydraulic control system. The decoupling problem of the servo controller needs to be considered, which is completed in the following chapters.

3. Decoupling Design of the Servo Controller

As mentioned in Section 2.3, the servo controller consists of two parts: an integral link and a stabilizing link. For hydraulic control systems, these two links can only be realized through hydraulic components. The design processes are detailed below.

3.1. Integral Controller

3.1.1. Characteristics Analysis of the Servo Valve

The nonlinear dynamic equation for the servo valve is:

$$A_y P_S - A_y P_C - F_L - M_y \ddot{x}_y - K_{f1} \dot{x}_y - K_1 x_y = 0 \tag{17}$$

where M_y is the mass, K_1 is the spring stiffness, K_{f1} is the viscous friction coefficient, and F_L is the initial spring force.

The relevant linear dynamic differential equation is:

$$A_y \cdot (\Delta P_S - \Delta P_C) - M_y \cdot \Delta \ddot{x}_y - K_{f1} \cdot \Delta \dot{x}_y - K_1 \cdot \Delta x_y = 0 \tag{18}$$

Its steady-state characteristic is:

$$\Delta x_y = -\frac{A_y}{K_1}(\Delta P_C - \Delta P_S) \tag{19}$$

Obviously, the steady-state value of Δx_y reflects the tracking error.

3.1.2. Characteristics Analysis of the Adjusting Chamber

The pressure–flow nonlinear dynamic equation of the adjusting pressure is:

$$\frac{dP_Z}{dt} = \frac{B}{V_Z} \cdot \left(C_{qin} A_{in} \sqrt{\frac{2(P_S - P_Z)}{\rho}} - C_{qout} A_{out} \sqrt{\frac{2(P_Z - P_T)}{\rho}} - A_{zx} \dot{x}_z \right) \tag{20}$$

The relevant linear dynamic differential equation is:

$$\Delta \dot{P}_Z = \frac{B}{V_Z} \cdot \left(-(K_{PY} + K_{PT2}) \cdot \Delta P_Z + K_{AY} \cdot \Delta A_{in} - K_{AT2} \cdot \Delta A_{out} + K_{PY} \cdot \Delta P_S - A_{zx} \cdot \Delta \dot{x}_z \right) \tag{21}$$

where $K_{AY} = C_{qin} \sqrt{\frac{2(P_S - P_Z)}{\rho}}$, $K_{PY} = C_{qin} A_{in} \sqrt{\frac{1}{2\rho(P_S - P_Z)}}$, $K_{AT2} = C_{qout} \sqrt{\frac{2(P_Z - P_T)}{\rho}}$, $K_{PT2} = C_{qout} A_{out} \sqrt{\frac{1}{2\rho(P_Z - P_T)}}$.

The functions $A_{in} = f_{in}(x_{uin})$ and $A_{out} = f_{out}(x_{uout})$ are adopted to represent the geometry relationship of the servo valve inlet orifice and outlet orifice, respectively. According to their linearized gain characteristics:

$$\Delta A_{in} = \frac{df_{in}}{dx_{uin}} \cdot \Delta x_{uin}, \quad \Delta A_{out} = \frac{df_{out}}{dx_{uout}} \cdot \Delta x_{uout} \tag{22}$$

Since $\Delta x_{uin} = -\Delta x_{uout} = \Delta x_y$, then

$$\Delta A_{in} = \frac{df_{in}}{dx_{uin}} \cdot \Delta x_y, \quad \Delta A_{out} = -\frac{df_{out}}{dx_{uout}} \cdot \Delta x_y \tag{23}$$

If the steady-state servo inlet and outlet flow area are both designed as 0, that is $A_{in,0} = A_{out,0} = 0$, there are:

$$K_{PY} = 0, K_{PT2} = 0 \tag{24}$$

Then, it has:

$$\Delta \dot{P}_Z = \frac{B}{V_Z} \cdot \left(\left(K_{AY} \cdot \frac{df_{in}}{dx_{uin}} + K_{AT2} \cdot \frac{df_{out}}{dx_{uout}} \right) \cdot \Delta x_y - A_{zx} \cdot \Delta \dot{x}_z \right) \tag{25}$$

where the generalized integral control gain is defined as:

$$K_C = \frac{B}{V_Z} \cdot \left(K_{AY} \cdot \frac{df_{in}}{dx_{uin}} + K_{AT2} \cdot \frac{df_{out}}{dx_{uout}} \right) \tag{26}$$

Then, it has:

$$\Delta P_Z = \int \Delta \dot{P}_Z dt = K_C \int \Delta x_y dt - \frac{B}{V_Z} \cdot A_{zx} \cdot \Delta x_z \tag{27}$$

Because Δx_y reflects the tracking error ($\Delta P_C - \Delta P_S$), the integrator for the tracking error is embedded through Equation (27). Obviously, the integral function can be realized, and it ensures the performance of servo tracking without static error.

Finally, the state–space model of the integral controller is:

$$\begin{aligned} \dot{x}_i &= A_i x_i + B_i u_i \\ y_i &= C_i x_i + D_i u_i \end{aligned} \tag{28}$$

where $x_i = [\Delta x_y \quad \Delta \dot{x}_y \quad \Delta P_Z]^T$, $u_i = [e \quad \Delta \dot{x}_z]^T$, $y_i = [\Delta P_Z]$,

$$A_i = \begin{bmatrix} 0 & 1 & 0 \\ -\frac{K_1}{M_y} & -\frac{K_{f1}}{M_y} & 0 \\ K_C & 0 & 0 \end{bmatrix}, B_i = \begin{bmatrix} 0 & 0 \\ -\frac{A_y}{M_y} & 0 \\ 0 & -\frac{B}{V_Z} \cdot A_{zx} \end{bmatrix} \quad (29)$$

$$C_i = [0 \quad 0 \quad 1], D_i = [0 \quad 0]$$

3.2. Stabilizing Controller

The nonlinear dynamic equation of the adjusting valve is:

$$A_{zx}P_Z - A_{zx}P_C - M_z\ddot{x}_z - K_{f2}\dot{x}_z - K_2x_z - F_{L2} = 0 \quad (30)$$

where M_z is the mass, K_2 is the spring stiffness, K_{f2} is the viscous friction coefficient, and F_{L2} is the initial spring force.

The relevant linear dynamic differential equation is:

$$A_{zx} \cdot (\Delta P_Z - \Delta P_C) - M_z \cdot \Delta \ddot{x}_z - K_{f2} \cdot \Delta \dot{x}_z - K_2 \cdot \Delta x_z = 0 \quad (31)$$

Its steady-state characteristic is:

$$\Delta x_z = \frac{A_{zx}}{K_2} (\Delta P_Z - \Delta P_C) \quad (32)$$

Obviously, the steady-state value of Δx_z reflects the error e_u .

The function $A_Z = f_Z(x_{uz})$ is adopted to represent the geometry relationship of the adjusting valve orifice. Its linearized gain characteristic is:

$$\Delta A_Z = \frac{df_Z}{dx_{uz}} \cdot \Delta x_{uz} \quad (33)$$

Since $\Delta x_{uz} = -\Delta x_z$, then:

$$\Delta A_Z = -\frac{df_Z}{dx_{uz}} \cdot \Delta x_z \quad (34)$$

Because Δx_z reflects the error $(\Delta P_Z - \Delta P_C)$, the negative feedback function is embedded through Equation (34), and it ensures the robust asymptotic stability, as well as the disturbance rejection performance.

The generalized stabilizing control gain is defined as:

$$K_Z = \frac{df_Z}{dx_{uz}} \quad (35)$$

Finally, the state-space model of the stabilizing controller is:

$$\begin{aligned} \dot{x}_s &= A_s x_s + B_s u_s \\ y_s &= C_s x_s + D_s u_s \end{aligned} \quad (36)$$

where $x_s = [\Delta x_z \quad \Delta \dot{x}_z]^T$, $u_s = [e_u]$, $y_s = [\Delta A_Z]$,

$$A_s = \begin{bmatrix} 0 & 1 \\ -\frac{K_2}{M_z} & -\frac{K_{f2}}{M_z} \end{bmatrix}, B_s = \begin{bmatrix} 0 \\ \frac{A_{zx}}{M_z} \end{bmatrix} \quad (37)$$

$$C_s = [-K_Z \quad 0], D_s = [0]$$

3.3. State–Space Model of the Servo Controller

According to the aforementioned content, the structure of the decoupling controllers is shown in Figure 5.

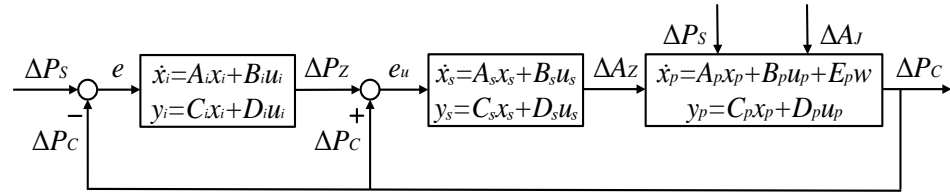


Figure 5. Structure diagram of the decoupling controllers.

Combining the integral link and the stabilization link, the state–space model of the servo controller can be expressed as:

$$\begin{aligned} \dot{x}_c &= A_c x_c + B_{c1} y + B_{c2} r \\ u &= C_c x_c + D_{c1} y + D_{c2} r \end{aligned} \tag{38}$$

where $x_c = [\Delta x_y \quad \Delta \dot{x}_y \quad \Delta P_Z \quad \Delta x_z \quad \Delta \dot{x}_z]^T$, $y = [\Delta P_C]$, $r = [\Delta P_S]$, $u = [\Delta A_Z]$,

$$A_c = \begin{bmatrix} 0 & 1 & 0 & 0 & 0 \\ -\frac{K_1}{M_y} & -\frac{K_{f1}}{M_y} & 0 & 0 & 0 \\ K_C & 0 & 0 & 0 & -\frac{B}{V_Z} \cdot A_{zx} \\ 0 & 0 & 0 & 0 & 1 \\ 0 & 0 & \frac{A_{zx}}{M_z} & -\frac{K_2}{M_z} & -\frac{K_{f2}}{M_z} \end{bmatrix}, B_{c1} = \begin{bmatrix} 0 \\ -\frac{A_y}{M_y} \\ 0 \\ 0 \\ -\frac{A_{zx}}{M_z} \end{bmatrix}, B_{c2} = \begin{bmatrix} 0 \\ \frac{A_y}{M_y} \\ 0 \\ 0 \\ 0 \end{bmatrix} \tag{39}$$

$$C_c = [0 \quad 0 \quad 0 \quad -K_Z \quad 0], D_{c1} = [0], D_{c2} = [0]$$

Then, the integrated structure of the servo controller is shown in Figure 6.

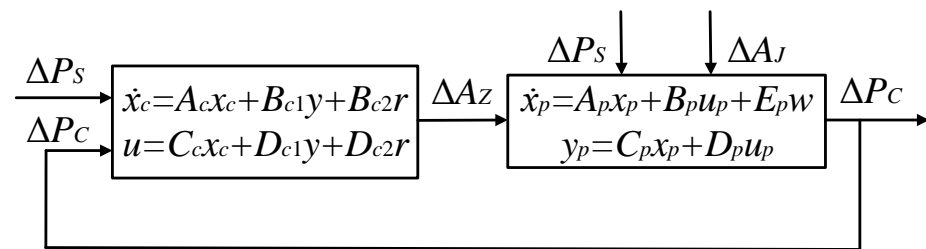


Figure 6. Integrated structure diagram of the servo controller.

4. Robust LQR Design Method

As mentioned in Section 3.1.2, the steady-state flow area of the servo inlet and outlet orifices are both designed as 0. It follows that once the flow area variation gradient of the orifice is determined, the generalized integral control gain K_C is a constant value at any steady-state working point and cannot be designed arbitrarily.

When combining the servo controller and the controlled plant, embedding the generalized integral control gain K_C in the state–space model, and considering the generalized stabilizing control gain K_Z as the static output feedback gain, the open-loop augmented state–space model of the whole system can be expressed as:

$$\begin{aligned} \dot{x} &= Ax + Bu + Ew \\ y &= Cx + Du \end{aligned} \tag{40}$$

where $x = [\Delta x_y \quad \Delta \dot{x}_y \quad \Delta P_Z \quad \Delta x_z \quad \Delta \dot{x}_z \quad \Delta P_C \quad \Delta P_O]^T$, $u = [\Delta A_Z]$, $y = [\Delta x_z]$,

$$\begin{aligned}
 A &= \begin{bmatrix} 0 & 1 & 0 & 0 & 0 & 0 & 0 \\ -\frac{K_1}{M_y} & -\frac{K_{f1}}{M_y} & 0 & 0 & 0 & -\frac{A_y}{M_y} & 0 \\ K_C & 0 & 0 & 0 & -\frac{B}{V_Z} \cdot A_{zx} & 0 & 0 \\ 0 & 0 & 0 & 0 & 1 & 0 & 0 \\ 0 & 0 & \frac{A_{zx}}{M_z} & -\frac{K_2}{M_z} & -\frac{K_{f2}}{M_z} & -\frac{A_{zx}}{M_z} & 0 \\ 0 & \frac{B}{V_C} \cdot A_y & 0 & 0 & \frac{B}{V_C} \cdot A_{zx} & -\frac{B}{V_C} \cdot (K_{PJ} + K_{PZ}) & \frac{B}{V_C} \cdot K_{PZ} \\ 0 & 0 & 0 & 0 & 0 & \frac{B}{V_O} \cdot K_{PZ} & -\frac{B}{V_O} \cdot (K_{PZ} + K_{PT}) \end{bmatrix} \\
 B &= \begin{bmatrix} 0 \\ 0 \\ 0 \\ 0 \\ 0 \\ -\frac{B}{V_C} \cdot K_{AZ} \\ \frac{B}{V_O} \cdot K_{AZ} \end{bmatrix}, E = \begin{bmatrix} 0 & 0 \\ 0 & \frac{A_y}{M_y} \\ 0 & 0 \\ 0 & 0 \\ 0 & 0 \\ \frac{B}{V_C} \cdot K_{AJ} & \frac{B}{V_C} \cdot K_{PJ} \\ 0 & 0 \end{bmatrix} \\
 C &= [0 \ 0 \ 0 \ 1 \ 0 \ 0 \ 0], D = [0]
 \end{aligned} \tag{41}$$

This is a typical static output feedback design problem, and its output feedback control law is:

$$u = -K_Z \cdot y \tag{42}$$

The topology of the output feedback control system is shown in Figure 7.

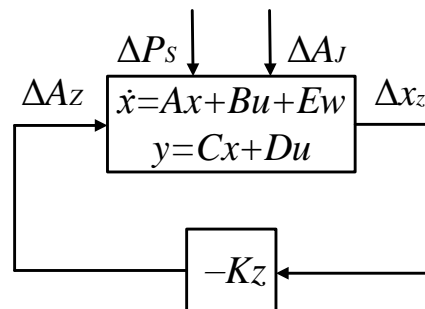


Figure 7. Topology of the output feedback control system.

4.1. Output Feedback Control Gains Design

4.1.1. Integral Control Gain

Defined as:

$$\frac{df_{in}}{dx_{uin}} \in [k_{in,min}, k_{in,max}], \frac{df_{out}}{dx_{uout}} \in [k_{out,min}, k_{out,max}] \tag{43}$$

where $k_{in,min}$, $k_{in,max}$, $k_{out,min}$ and $k_{out,max}$ is the extremum values of the flow area variation gradient of the servo inlet orifice and outlet orifice, respectively.

According to Equation (26), it has:

$$K_C \in \left[\frac{B}{V_Z} \cdot (K_{AY} \cdot k_{in,min} + K_{AT2} \cdot k_{out,min}), \frac{B}{V_Z} \cdot (K_{AY} \cdot k_{in,max} + K_{AT2} \cdot k_{out,max}) \right] \tag{44}$$

According to the structural parameter limitations, appropriate values of the flow area variation gradient can be designed, then the integral control gain can be determined.

4.1.2. Stabilization Control Gain

The quadratic optimization objective for Equation (40) is defined as:

$$J = \frac{1}{2} \int_0^{\infty} [y^T \cdot Q \cdot y + u^T \cdot R \cdot u] dt \quad (45)$$

where $Q = Q^T \geq 0$, $R = R^T > 0$.

Then, the LQR state feedback control law is:

$$u = -K_x \cdot x = -R^{-1} B^T P \cdot x \quad (46)$$

where K_x is the state feedback control gain vector, and P is the solution of an ARE algebraic equation, expressed as:

$$PA + A^T P + C^T Q C - P B R^{-1} B^T P = 0 \quad (47)$$

By designing the weight matrices Q and R to optimize the quadratic objective, a positive definite solution P of the ARE equation can be obtained. Then, the above system yields satisfactory closed-loop reference dynamics, described by:

$$\dot{x} = (A - B K_x) x = F x \quad (48)$$

Using the output feedback control law expressed by Equation (42), the dominant eigenvalue Λ_1 and its associated eigenvector X_1 of the state feedback design can be retained, and the static output feedback gain is given by [3]:

$$K_Z = K_x X_1 (C X_1)^{-1} \quad (49)$$

where the eigenvector X_1 and the eigenvalue Λ_1 satisfy the eigen equation for the state feedback system, described as:

$$F X_1 = X_1 \Lambda_1 \quad (50)$$

Finally, the closed-loop system is calculated as:

$$\dot{x} = (A - B K_Z C) x = A_{cl} x \quad (51)$$

4.2. Design and Implementation Method of the Servo Controller

Assuming that the performance requirements are:

1. Steady-state requirement: The steady-state pressure drop is designed as P_e , and the phase margin should be more than N° ;
2. Dynamic requirement: The settling time should be within the t_s , and the overshoot should be within the σ .

4.2.1. Control Gains Design

The steady-state flow balance equation of the controlled plant is:

$$(C_{qj} A_J + C_{q1} A_1) \sqrt{\frac{2(P_S - P_C)}{\rho}} = C_{qz} A_Z \sqrt{\frac{2(P_C - P_O)}{\rho}} = C_{q0} A_2 \sqrt{\frac{2(P_O - P_T)}{\rho}} \quad (52)$$

At a steady-state working point, if the inlet pressure is represented as $P_{S,i}$, and the metered flow area is represented as $A_{J,i}$, then:

$$P_{C,i} = P_{S,i} - P_e \quad (53)$$

$$P_{O,i} = \left(\frac{C_{qj,i}A_{J,i} + C_{q1,i}A_1}{C_{qo,i}A_2} \right)^2 \cdot (P_{S,i} - P_{C,i}) + P_T \quad (54)$$

$$A_{Z,i} = \left(\frac{C_{qj,i}A_{J,i} + C_{q1,i}A_1}{C_{qz,i}} \right) \sqrt{\frac{(P_{S,i} - P_{C,i})}{(P_{C,i} - P_{O,i})}} \quad (55)$$

Subsequently, the parameters $K_{AJ,i}$, $K_{AZ,i}$, $K_{PZ,i}$, $K_{PJ,i}$ and $K_{PT,i}$ can be calculated. The steady-state balance equation of the adjusting valve is:

$$0 = A_{zx}P_{C,i} - A_{zx}P_{Z,i} - K_2x_{szd,i} \quad (56)$$

Then:

$$P_{Z,i} = P_{C,i} + \frac{K_2}{A_{zx}} \cdot x_{szd,i} \quad (57)$$

Subsequently, the parameters $K_{AY,i}$ and $K_{AT2,i}$ can be calculated.

When designing appropriate values of the flow area variation gradient $\frac{df_{in}}{dx_{uj,i}}$ and $\frac{df_{out}}{dx_{uout}}$, then the integral control gain K_C can be determined according to Equation (26).

When designing optimized weight matrices Q and R that meet the above performance requirements, a positive definite solution P_i of the ARE equation can be obtained, and the state feedback control gain vector $K_{x,i}$ can be obtained, then the stabilization control gain is expressed as:

$$K_{Z,i} = K_{x,i}X_1(CX_1)^{-1} \quad (58)$$

4.2.2. Orifice Geometry Relationship Design

A design formula is provided to deal with the geometry relationship design problem of the flow area increment ($A_{Z,i} - A_{Z,i-1}$) and the orifice underlap increment $\Delta x_{uz,i}$, expressed by:

$$\Delta x_{uz,i} = \frac{(A_{Z,i} - A_{Z,i-1})}{K_{Z,i-1}}, i = 2, 3, \dots, N \quad (59)$$

where N is the number of the designed steady-state working points [24].

Assuming that the adjusting valve steady-state spring compression at the $(i - 1)$ -th steady-state working point is $x_{szd,i-1}$, then the calculation formula of the steady-state spring compression at the i -th steady-state working point is provided as:

$$x_{szd,i} = x_{szd,i-1} + \Delta x_{uz,i} \quad (60)$$

4.2.3. Valve Initial Parameters Design

(1) Adjusting valve

The initial underlap and the underlap at the first steady-state working point are designed as $x_{uz,0}$ and $x_{uz,1}$, respectively. Since $\Delta x_{uz} = \Delta x_{szd}$, the initial spring compression $x_{szd,0}$ is calculated as:

$$x_{szd,0} = x_{szd,1} - (x_{uz,1} - x_{uz,0}) \quad (61)$$

(2) Servo valve

The steady-state balance equation of the servo valve is:

$$0 = A_y P_{S,i} - A_y P_{C,i} - Kx_{scd,i} \quad (62)$$

Then, at the first steady-state working point, the steady-state spring compression is:

$$x_{scd,1} = \frac{A_y}{K} P_e \quad (63)$$

The initial underlap and the underlap at the first steady-state working point is designed as $x_{uin,0}$ and $x_{uin,1}$, respectively. Since $\Delta x_{uin} = \Delta x_{scd}$, the initial spring compression $x_{scd,0}$ is calculated as:

$$x_{scd,0} = x_{scd,1} - (x_{uin,1} - x_{uin,0}) \tag{64}$$

5. Design Example

The structural parameters of the pressure drop control valve are shown in Table 1.

Table 1. Structural parameters of the pressure drop control valve.

Parameter/Unit	Value	Parameter/Unit	Value
M_y /Kg	0.08	K_1 /(N/m)	4×10^4
M_z /Kg	0.05	K_{f1} /(N/(m/s))	200
d_y /m	0.036	K_2 /(N/m)	1.5×10^4
d_z /m	0.036	K_{f2} /(N/(m/s))	200
V_C /m ³	2×10^{-6}	ρ /(Kg/m ³)	780
V_Z /m ³	2×10^{-6}	B /MPa	1.7×10^3
V_O /m ³	4.9087×10^{-4}	C_{qmax}	0.7
A_1 /m ²	2.8274×10^{-7}	Nu /Pas	0.051
A_2 /m ²	1.9007×10^{-4}	$lamc$	1×10^3
P_T /MPa	0.2		

The input conditions include:

1. The inlet pressure P_S is within [3, 9] the MPa;
2. The metered flow area A_J is within $[10, 240] \times 10^{-6} \text{ m}^2$.

The design objectives include:

1. Geometry design of the adjusting orifice $A_Z = f_Z(x_{uz})$;
2. Geometry design of the servo orifices $A_{in} = f_{in}(x_{uin})$ and $A_{out} = f_{out}(x_{uout})$.

The performance requirements include:

1. The rated pressure drop P_e is 0.92 MPa, and the variation range is within 0.01 MPa;
2. The settling time is within 0.01 s, and the overshoot is within 10%;
3. The phase margin should be more than 50°.

5.1. Dynamic Design

5.1.1. First Steady-State Working Point

The input conditions of the first steady-state working point are: the metered flow area $A_{J,1}$ is $10 \times 10^{-6} \text{ m}^2$, and the inlet pressure $P_{S,1}$ is 9 MPa. According to Equations (53)–(55), then:

$$P_{C,1} = P_{S,1} - \Delta P_e = 8.08 \text{ MPa} \tag{65}$$

$$P_{O,1} = \left(\frac{C_{qj,1}A_{J,1} + C_{q1,1}A_1}{C_{qo,1}A_2} \right)^2 \cdot (P_{S,1} - P_{C,1}) + P_T = 0.20265 \text{ MPa} \tag{66}$$

$$A_{Z,1} = \left(\frac{C_{qj,1}A_{J,1} + C_{q1,1}A_1}{C_{qz,1}} \right) \sqrt{\frac{(P_{S,1} - P_{C,1})}{(P_{C,1} - P_{O,1})}} = 3.48627 \cdot 10^{-6} \text{ m}^2 \tag{67}$$

Then, the parameters $K_{AJ,1}$, $K_{AZ,1}$, $K_{PZ,1}$, $K_{PJ,1}$ and $K_{PT,1}$ are calculated as:

$$K_{AJ,1} = C_{qj,1} \sqrt{\frac{2(P_{S,1} - P_{C,1})}{\rho}} = 33.99849 \tag{68}$$

$$K_{AZ,1} = C_{qz,1} \sqrt{\frac{2(P_{C,1} - P_{O,1})}{\rho}} = 99.48459 \tag{69}$$

$$K_{PZ,1} = C_{qz,1} A_{Z,1} \sqrt{\frac{1}{2\rho(P_{C,1} - P_{O,1})}} = 2.20144 \cdot 10^{-11} \tag{70}$$

$$K_{PJ,1} = (C_{qj,1} A_{J,1} + C_{q1,1} A_1) \sqrt{\frac{1}{2\rho(P_{S,1} - P_{C,1})}} = 1.88494 \cdot 10^{-10} \tag{71}$$

$$K_{PT,1} = C_{qo,1} A_2 \sqrt{\frac{1}{2\rho(P_{O,1} - P_T)}} = 6.54328 \cdot 10^{-8} \tag{72}$$

Designing the spring compression $x_{szd,1}$ as 10 mm. According to Equation (57), it has:

$$P_{Z,1} = P_{C,1} + \frac{K_2}{A_{zx}} \cdot x_{szd,1} = 8.22737 \text{ MPa} \tag{73}$$

Then, the parameters $K_{AY,1}$ and $K_{AT2,1}$ are calculated as:

$$K_{AY,1} = C_{qin,1} \sqrt{\frac{2(P_{S,1} - P_{Z,1})}{\rho}} = 31.15679 \tag{74}$$

$$K_{AT2,1} = C_{qout,1} \sqrt{\frac{2(P_{Z,1} - P_T)}{\rho}} = 100.42741 \tag{75}$$

When designing the weight matrices Q as 2.041 and R as 2000, the different control gain design schemes are shown in Table 2.

Table 2. Different control gain design schemes at the first steady-state working point.

$\frac{df_{in}}{dx_{uin}} / \frac{df_{out}}{dx_{uout}}$	$K_{Z,1}$	Phase/°
0.005	0.0213	60.4
0.010	0.0307	59.8
0.015	0.0303	59.0
0.020	0.0302	58.1
0.025	0.0289	57.2
0.030	0.0311	56.4
0.035	0.0318	55.6
0.040	0.0385	55.0

5.1.2. Other Steady-State Working Points

In this paper, the flow area variation gradient of the servo inlet orifice and outlet orifice $\frac{df_{in}}{dx_{uin}}$ and $\frac{df_{out}}{dx_{uout}}$ are both designed as 0.03, and the 4×5 steady-state working points are selected as the designed points. Subsequently, when executing the design processes shown in Section 5.1.1, the stabilization control gains that meet the above performance requirements can be obtained, as shown in Table 3.

Table 3. Stabilization control gains at each steady-state working point.

P_S MPa	A_J mm ²	A_Z mm ²	K_Z	Phase/°
3	10	7.1413178	0.0305	69.2
	30	21.258905	0.0251	87.6
	80	58.720918	0.0161	89.4
	160	138.75330	0.0299	83.1
	240	359.53286	0.0305	89.8

Table 3. Cont.

P_S MPa	A_J mm ²	A_Z mm ²	K_Z	Phase/°
5	10	4.9691655	0.0302	61.5
	30	14.750547	0.0288	84.5
	80	39.904931	0.0151	84.5
	160	85.546194	0.0201	76.0
	240	148.38949	0.0259	70.4
7	10	4.0360839	0.0298	58.2
	30	11.969912	0.0301	82.6
	80	32.175269	0.0152	81.1
	160	67.213819	0.0141	73.7
	240	109.70300	0.0159	68.5
9	10	3.4862689	0.0311	56.4
	30	10.334703	0.0281	81.3
	80	27.693258	0.0221	76.6
	160	57.160884	0.0121	70.7
	240	90.995231	0.0149	62.8

5.1.3. Valve Initial Parameters Design

(1) Adjusting valve

The initial underlap $x_{uz,0}$ and the underlap at the first steady-state working point $x_{uz,1}$ are both designed as 0.1 mm. According to Equation (61), it has:

$$x_{szd,0} = x_{szd,1} - (x_{uz,1} - x_{uz,0}) = 10 \text{ mm} \quad (76)$$

(2) Servo valve

According to Equation (63), at the first steady-state working point, the steady-state spring compression is:

$$x_{scd,1} = \frac{A_y}{K} P_e = 23.39155 \text{ mm} \quad (77)$$

The initial underlap $x_{uin,0}$ and the underlap at the first steady-state working point $x_{uin,1}$ are both designed as 0 mm. According to Equation (64), it has:

$$x_{scd,0} = x_{scd,1} - (x_{uin,1} - x_{uin,0}) = 23.39155 \text{ mm} \quad (78)$$

Finally, the summary of the designed initial parameters is shown in Table 4.

Table 4. Summary table of the designed initial parameters.

Parameter/Unit	Value
$x_{szd,0}$ /mm	10
$x_{scd,0}$ /mm	23.39155
$x_{uz,0}$ /mm	0.1
$x_{uin,0}$ /mm	0
$x_{uout,0}$ /mm	0

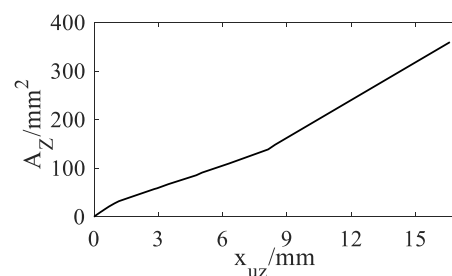
5.1.4. Orifice Geometry Relationship Design

According to Equations (59) and (60), the geometry relationship value pair of the adjusting orifice is shown in Table 5.

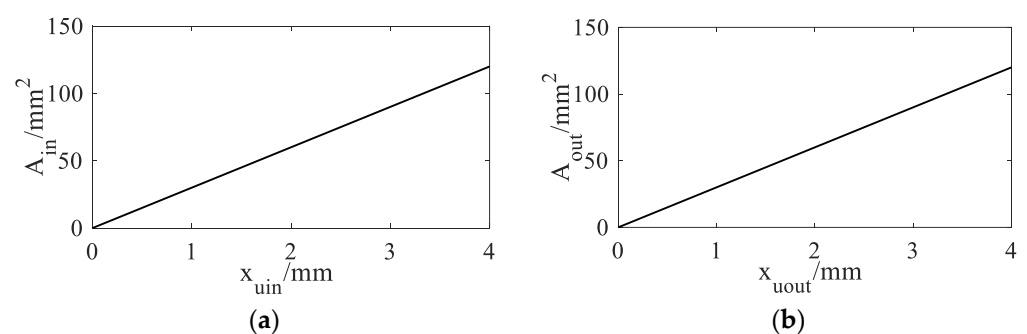
Table 5. Geometry relationship value pair of the adjusting orifice.

x_{uz} mm	A_z mm ²
0	0
0.1	3.4862689
0.117678939	4.0360839
0.148990402	4.9691655
0.220915975	7.1413178
0.325617129	10.334703
0.38380962	11.969912
0.47618952	14.750547
0.702174173	21.258905
0.958522898	27.693258
1.161328826	32.175269
1.669859221	39.904931
2.812637565	57.160884
2.941565995	58.720918
3.469075374	67.213819
4.769243813	85.546194
5.040340181	90.995231
6.295895148	109.70300
8.122958041	138.75330
8.445238643	148.38949
16.59749231	359.53286

Moreover, the geometry relationship diagram of the adjusting orifice is shown in Figure 8.

**Figure 8.** Geometry relationship diagram of the adjusting orifice.

In addition, the geometry relationship diagrams of the servo inlet orifice and outlet orifice are shown in Figure 9a,b.

**Figure 9.** (a) Geometry relationship diagram of the servo inlet orifice; (b) geometry relationship diagram of the servo outlet orifice.

5.2. Simulation and Discussion

A nonlinear model is established based on the AMESim software, and the structure diagram is shown in Figure 10.

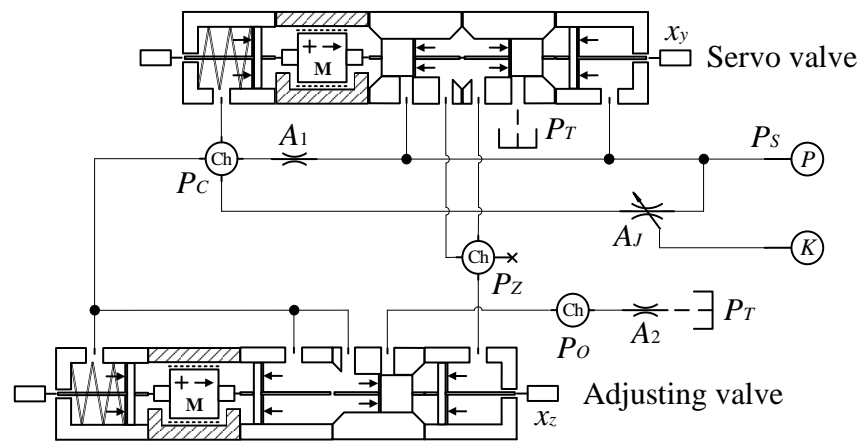


Figure 10. Structure diagram of the nonlinear model.

According to Table 1, the relevant structure parameters are set, and according to Table 4, the relevant initial parameters are set. In addition, the remaining structure parameters and the simulation parameters are set to the default values of AMESim.

5.2.1. Simulation

Executing the following simulation tasks, the performance of the designed system can be verified. The input conditions and the simulation results are detailed below.

1. The step signal of the inlet pressure P_S is shown in Figure 11. Besides, the steady-state working points of the metered flow area A_J are designed as 10 mm^2 , 50 mm^2 , 100 mm^2 , 150 mm^2 , 200 mm^2 , and 240 mm^2 , respectively. The simulation results are shown in Figure 12.

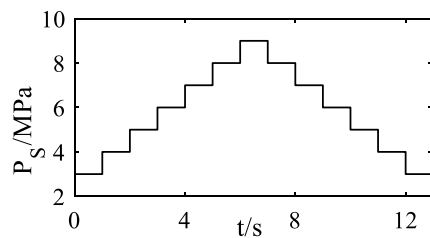


Figure 11. Step signal of the inlet pressure.

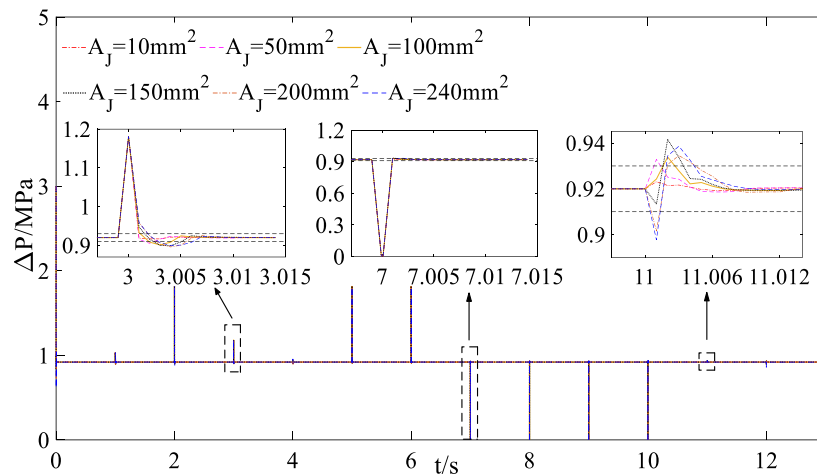


Figure 12. Response curves when the inlet pressure changes.

- The step signal of the metered flow area A_f is shown in Figure 13. Besides, the steady-state working points of the inlet pressure P_S are designed as 3 MPa, 4 MPa, 5 MPa, 6 MPa, 7 MPa, 8 MPa, and 9 MPa, respectively. The simulation results are shown in Figure 14.

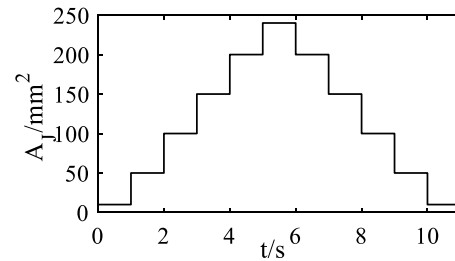


Figure 13. Step signal of the metered flow area.

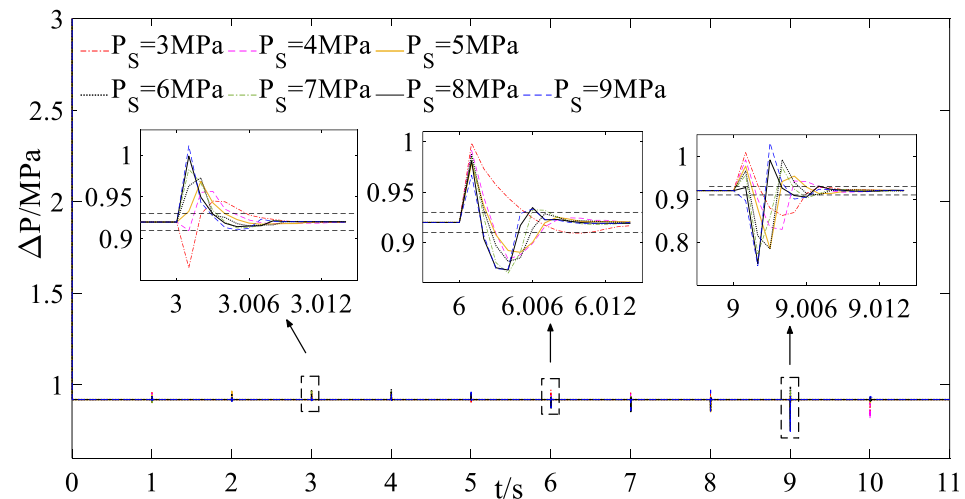


Figure 14. Response curves when the metered flow area disturbs.

5.2.2. Discussion

The simulation results shown in Figures 12 and 14 indicate that:

- Despite suffering from strong step inputs, the controlled pressure drop is always 0.92 MPa, and the static error is almost 0. Evidently, the designed control device has the ability to perform servo tracking without static error. It follows that the theoretical design architecture is relevant and the LQR design method is effective;
- During each transient process, the settling time is within 0.01s and the dynamic overshoot is within 10%. Obviously, the dynamic performances match the design requirements. It follows that the derived models are precise and the designed weight matrices, Q and R, are reasonable.

In addition, although the proposed method is based on the linear model, the designed system still has good performance and strong robustness when faced with nonlinear effects, such as leakage. The verification processes are detailed below.

According to the aforementioned content, the adjusting chamber is almost dead at each steady-state working point, hence it is most likely to leak. Assuming that the adjusting chamber leaks, a nonlinear model can be established, and the structure diagram is shown in Figure 15.

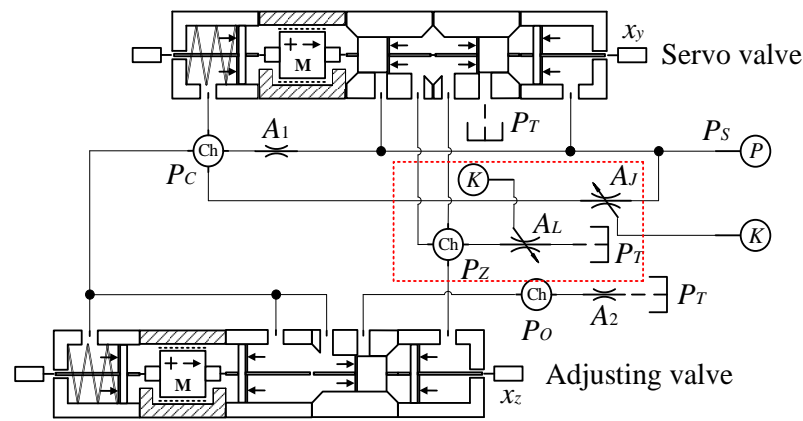


Figure 15. Structure diagram of the nonlinear model when the adjusting chamber leaks.

The leakage area is represented as A_L , and it is designed as 0 mm^2 , 0.5 mm^2 , 1.0 mm^2 , 1.5 mm^2 , 2.0 mm^2 , and 2.5 mm^2 , respectively. Selecting some steady-state working points for verification and executing the following simulation tasks:

1. The step signal of the inlet pressure P_S is still shown in Figure 11 and the metered flow area A_J is designed as 150 mm^2 . The simulation results are shown in Figure 16;
2. The step signal of the metered flow area A_J is still shown in Figure 13 and the inlet pressure P_S is designed as 7 MPa . The simulation results are shown in Figure 17.

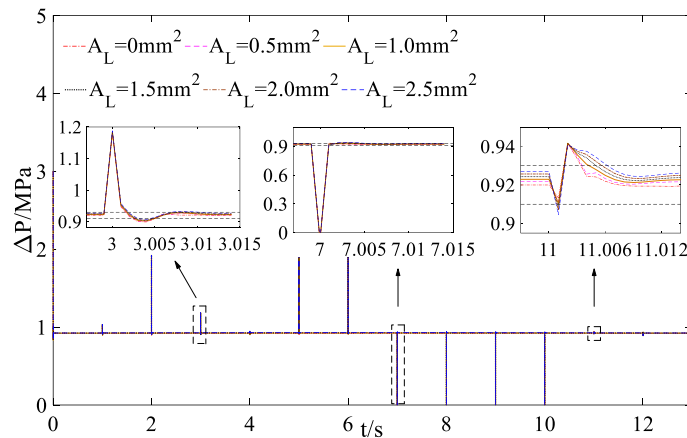


Figure 16. Response curves of the step in inlet pressure when the adjusting chamber leaks.

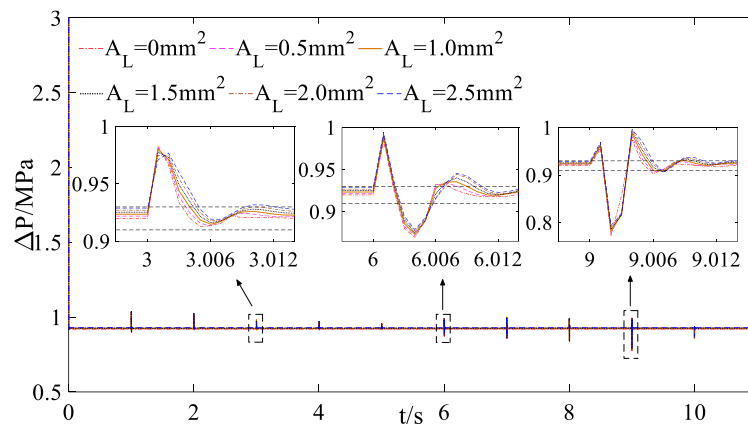


Figure 17. Response curves of the step in metered flow area when the adjusting chamber leaks.

The simulation results shown in Figures 16 and 17 indicate that:

1. When the adjusting chamber leaks, the pressure drop in the system deviates from the design value, and as the leakage area increases, the deviation increases; however, even if the leakage area reaches 2.5 mm^2 , the deviation is still within 0.01 MPa . Thus, the steady-state performance is acceptable;
2. Besides, during each transient process, the settling time is still within 0.01 s and the dynamic overshoot is still within 10% . Obviously, the dynamic performances match the design requirements and the leakage has a small impact on the dynamic performances.

To enhance the reliability of the simulation results, the same input conditions as mentioned in Section 5.2.1 are used and the leakage area is set as 2.5 mm^2 . When executing corresponding simulation tasks, the simulation results are shown in Figures 18 and 19.

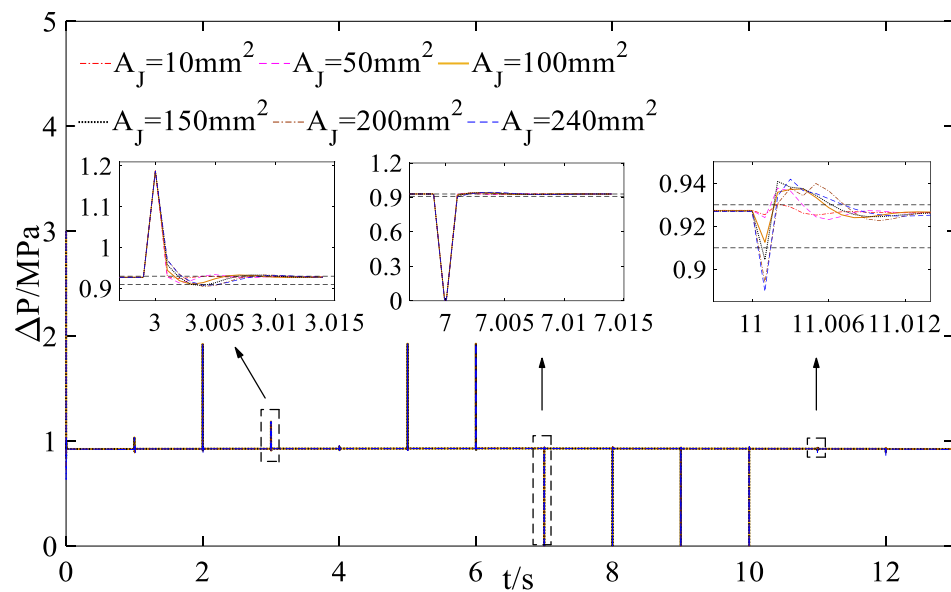


Figure 18. Response curves when the inlet pressure changes in the 2.5 mm^2 leakage area.

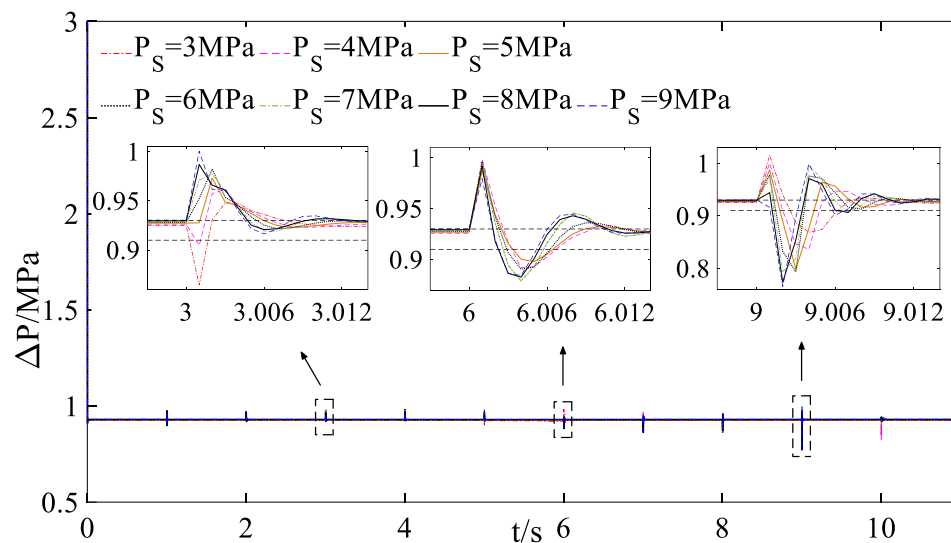


Figure 19. Response curves when the metered flow area is disturbed in the 2.5 mm^2 leakage area.

The simulation results indicate that the pressure drop in the system deviates from the design value, but the deviation is all within 0.01 MPa , and the designed system still has good steady-state and dynamic performance.

These simulation results show that, when faced with nonlinear effects, the designed system has strong robustness, and the proposed method is robust and effective.

6. Conclusions

In this paper, with the design object of achieving servo tracking without static error, an integral constant pressure drop control valve is designed, and a robust LQR design method is proposed. The conclusions are as follows:

1. Based on the servo system design theory, a servo control architecture for the pressure drop control valve is constructed and implemented, which can clearly explain the design theory of the system. In addition, the control architecture clearly displays the key structural design parameters, including the generalized stabilization control gain and the generalized servo control gain. Compared with classic design methods, the proposed design architecture and design method are more illustrative;
2. Based on the output feedback design theory, the robust LQR design method can realize the design of the key structural design parameters effectively and obtain optimized structural parameters to guarantee high precision and high robustness in performance. The proposed method provides more accurate guidance for the design of the structural parameters and improves the design efficiency;
3. The simulation results show that the designed integral constant pressure drop control valve has dual control functions of integral control and stabilization control and can realize tracking without static error and pretty good dynamic performance. Besides, when faced with nonlinear effects, the designed system still has good performance and strong robustness. Evidently, the proposed design method is robust and effective, and can also be used in the design process of other fuel system components.

However, nonlinearities also play an essential role in the design process, and it is meaningful to study how nonlinear characteristics affect system performance in a future study. Besides, if executing physical tests, the proposed design methods may not perform as well as the simulation results, which should also be tested in future work.

Author Contributions: Methodology, W.Z.; formal analysis, W.Z.; writing—original draft preparation, W.Z.; writing—review and editing, X.W.; validation, Y.L.; funding acquisition, Z.Z. and L.T. All authors have read and agreed to the published version of the manuscript.

Funding: This study was supported by the National Science and Technology Major Project (J2019-V-0010-0104).

Data Availability Statement: The data used to support the findings in this paper are contained in the text.

Conflicts of Interest: There are no conflict of interest.

References

1. Wu, D.G. *Research on the Performance of Turbofan Engine and Its System*; National Defense Industry Press: Beijing, China, 1986; pp. 161–201.
2. Wang, X.; Yang, S.B.; Zhu, M.Y.; Kong, X.X. *Aeroengine Control Principles*; Science Press: Beijing, China, 2021; pp. 128–257.
3. Lavretsky, E.; Wise, K.A. *Robust and Adaptive Control with Aerospace Applications*; Springer: London, UK, 2012; pp. 27–72. [[CrossRef](#)]
4. Yang, F.; Wang, X.; Cheng, T.; Liu, X. Dynamic characteristics analysis of a pressure differential valve. *Aeroengine* **2015**, *41*, 44–50. [[CrossRef](#)]
5. Ma, C.Y. The analysis and design of hydraulic pressure-reducing valves. *J. Eng. Ind.* **1967**, *89*, 301. [[CrossRef](#)]
6. Fan, R.; Zhang, M. The establishment of pilot-operated relief valve's dynamic mathematic model and the dynamic properties analysis. *J. ZhengZhou Text. Inst.* **1997**, *3*, 58–61.
7. Wu, D.; Burton, R.; Schoenau, G.; Bitner, D. Analysis of a pressure—Compensated flow control valve. *J. Dyn. Syst. Meas. Control.* **2007**, *129*, 203–211. [[CrossRef](#)]
8. Wen, Y.J. Analysis of characteristics of oil return differential pressure valve with EASY5. In Proceedings of the 11th Symposium on Automatic Engine Control of CAA, Beijing, China, 8–10 November 2002; pp. 21–26.
9. Hong, W.; Liu, H.L.; Wang, G.Z.; Qin, J. Research on pressure characteristics of relief valve without pressure overshoot. *Chin. Hydraul. Pneum.* **2012**, *10*, 104–106. [[CrossRef](#)]

10. Shang, Y.; Guo, Y.Q.; Wang, L. Study of impact of design parameter of differential pressure controller on fuel metering system. *Aeronaut. Manuf. Technol.* **2013**, *6*, 89–91. [[CrossRef](#)]
11. Wang, B.; Zhao, H.C.; Ye, Z.F. AMESim simulation of afterburning metering unit for fuel system. *Aeroengine* **2014**, *40*, 62–66. [[CrossRef](#)]
12. Hang, J.; Li, Y.Y.; Yang, L.M.; Li, Y.H. Design and Simulation of Large Flowrate Fuel Metering Valve of Aero engine Based on AMESim. In Proceedings of the 2020 15th IEEE Conference on Industrial Electronics and Applications (ICIEA), Kristiansand, Norway, 9–13 November 2020; IEEE: Piscataway, NJ, USA, 2020. [[CrossRef](#)]
13. Wei, Y.Y.; Wang, H.Y.; Miao, W.B. Analysis on modeling of constant pressure difference valve for a turboshaft engine. *Aeroengine* **2014**, *40*, 75–78. [[CrossRef](#)]
14. Zeng, D.T.; Wang, X. Design and analysis of characteristics of damping hole for a fuel metering valve. In Proceedings of the 2010 International Conference on Mechanical and Electrical Technology, Kyoto, Japan, 1–3 August 2010; IEEE: Piscataway, NJ, USA, 2010. [[CrossRef](#)]
15. Zeng, D.T.; Wang, X.; Tan, D.L.; Xu, M. Fuel scavenger contour performance analysis of fuel metering devices. *Aeroengine* **2010**, *36*, 38. [[CrossRef](#)]
16. Zeng, D.T.; Wang, X.; Tan, D.L. Effects of fuel returned shape on metering devices characteristics. *Aeroengine* **2012**, *38*, 46. [[CrossRef](#)]
17. Maiti, R.; Pan, S.; Bera, D. Analysis of a load sensing hydraulic flow control valve. *Proc. JFPS Int. Symp. Fluid Power* **1996**, *1996*, 307–312. [[CrossRef](#)]
18. Amirante, R.; Vescovo, G.D.; Lippolis, A. Flow forces analysis of an open center hydraulic directional control valve sliding spool. *Energy Convers. Manag.* **2006**, *47*, 114–131. [[CrossRef](#)]
19. Amirante, R.; Vescovo, G.D.; Lippolis, A. Evaluation of the flow forces on an open centre directional control valve by means of a computational fluid dynamic analysis. *Energy Convers. Manag.* **2006**, *47*, 1748–1760. [[CrossRef](#)]
20. Okungbowa, B.; Stanley, N. CFD Analysis of Steady State Flow Reaction Forces in a Rim Spool Valve. Master's Thesis, University of Saskatchewan, Saskatoon, SK, Canada, 2006.
21. Valdes, J.R.; Miana, M.J.; Nunez, J.L. Reduced order model for estimation of fluid flow and flow forces in hydraulic proportional valves. *Energy Convers. Manag.* **2008**, *49*, 1517–1529. [[CrossRef](#)]
22. Li, Z.; Guo, Y.Q.; Liao, G.H. Structure design and performance calculation of a differential pressure measuring device. In Proceedings of the 12th Engine Automatic Control Academic Conference of CAAC, Hong Kong, China, 1–5 November 2004; pp. 158–162.
23. Deng, Z.J.; Guo, L.Y. Analysis of speed fluctuation in bench test of aero-engine numerical control system. *China Sci. Technol. Overv.* **2020**, *15*, 63–65.
24. Zhao, W.; Wang, X.; Long, Y.; Zhou, Z.; Tian, L. Frequency Domain Design Method of the Aeroengine Fuel Servo Constant Pressure Difference Control System with High Performance. *Aerospace* **2022**, *9*, 775. [[CrossRef](#)]
25. Merritt, H.E. *Hydraulic Control Systems*; John Wiley: New York, NY, USA, 1967; pp. 360–374. [[CrossRef](#)]
26. Fitch, E.C.; Hong, I.T. *Hydraulic Component Design and Selection*; Barden Incorporated: Etobicoke, ON, Canada, 2004; pp. 205–213.
27. Li, C.G.; He, Y.M. *Modeling and Simulation Analysis of Hydraulic System*; Aviation Industry Press: Beijing, China, 2008; pp. 2–11.
28. Wang, Y.; Fan, D.; Zhang, C.; Peng, K.; Shi, D.Y. Design and analysis of the variable pressure-drop fuel metering device. In Proceedings of the 36th Chinese Control Conference, Dalian, China, 26–28 July 2017; pp. 6434–6439.
29. Agh, S.M.; Pirkandi, J.; Mahmoodi, M.; Jahromi, M. Optimum design simulation and test of a new flow control valve with an electronic actuator for turbine engine fuel control system. *Flow Meas. Instrum.* **2019**, *65*, 65–77. [[CrossRef](#)]
30. Yuan, Y.; Zhang, T.H.; Lin, Z.L.; Zhang, J.M. An investigation into factors determining the metering performance of a fuel control unit in an aero engine. *Flow Meas. Instrum.* **2020**, *71*, 101672. [[CrossRef](#)]

Disclaimer/Publisher's Note: The statements, opinions and data contained in all publications are solely those of the individual author(s) and contributor(s) and not of MDPI and/or the editor(s). MDPI and/or the editor(s) disclaim responsibility for any injury to people or property resulting from any ideas, methods, instructions or products referred to in the content.